EVLA MEMO 53

A VIVALDI FOCAL PLANE ARRAY FOR EVLA

Walter Brisken

National Radio Astronomy Observatory

March 6, 2003

Abstract A focal plane array is investigated as a possible option for sub-GHz observing with the EVLA. The practical geometry considered here, while probably not optimal, has been found to be promising. Some aspects of the analysis are absent from this document. Currently, the far-field, infinite array radiation pattern is used for all elements of the array. Also only one polarization is considered, and the array is analyzed only for an infinitesimal bandwidth. The final choice for a low frequency system will ultimately be determined by weighing costs against performance of the candidate systems.

1 The EVLA low-frequency problem

One goal of the EVLA project is to provide continuous frequency coverage from 300 MHz or lower to 50 GHz. Frequencies between 1 and 50 GHz will be supported with secondary focus feeds. At a frequency of 1 GHz, the subreflector becomes 8 wavelengths across. Below this frequency, diffraction around the subreflector becomes substantial, reducing its efficiency and increasing the system temperature. Additionally, the feed cone needed for frequencies below 1 GHz would be too large to fit in the feed circle. As it is, the 1-2 GHz feed barely fits. A primary focus solution is likely needed for frequencies below 1 GHz.

2 Current VLA low frequency feeds

The VLA currently sports a 330 MHz crossed-dipole feed at "prime focus" and occasionally a 74 MHz crossed-dipole at "out-of-focus". Both systems use the subreflector as a backplane, making them inherently narrow-band. The subreflector cannot be pulled high enough to expose the true best-bit prime focus of the antenna. Single dipoles do not make great feeds for a prime focus system because their radiation patterns do not uniformly illuminate the primary. Additionally, the presence of these dipole feeds is thought to worsen the performance of the VLA at its higher frequencies. For these reasons it is essential to implement a better system for EVLA.

3 The baseline plan for EVLA

The baseline plan for the low frequency system presented in the EVLA Phase II proposal consists of a prime-focus cooled receiver covering 700 MHz to 1 GHz, and additional units to cover frequencies below 700 MHz. In order to put them at prime focus, the subreflector would be put on a pivoting mount (the FRRM). The other sides of this rotating mount would host the other low frequency feeds. An array such as the one descibed here may be used for 250 MHz to 700 MHz. The option would remain open for a dipole or ATA-style log-periodic array at even lower frequencies.

4 A focal plane array for EVLA

4.1 Focal plane array concept

One option for a replacement low frequency system is a phased array of receiving elements placed near the subreflector. The desire not to block the subreflector forces the focal plane array to be placed off axis, resulting in a telescope that points about 7.2° off axis (see Fig. 1). This causes only a modest 1% loss in effective collecting area due to projection. It also precludes observing within about 5° of the zenith. It,

however, opens up the possibility of observing within 3° of the horizon. The focal plane array must be large enough to receive the distorted illumination pattern of the off-axis source. This illumination pattern is considerably larger in area than the equivalent for an on-axis system. Because the subreflector cannot be pulled high enough to expose the prime focus, and based purely geometric considerations, it is obvious that the size of the illumination pattern for an array that is to be deployable immediately below the subreflector must be larger than the subreflector.

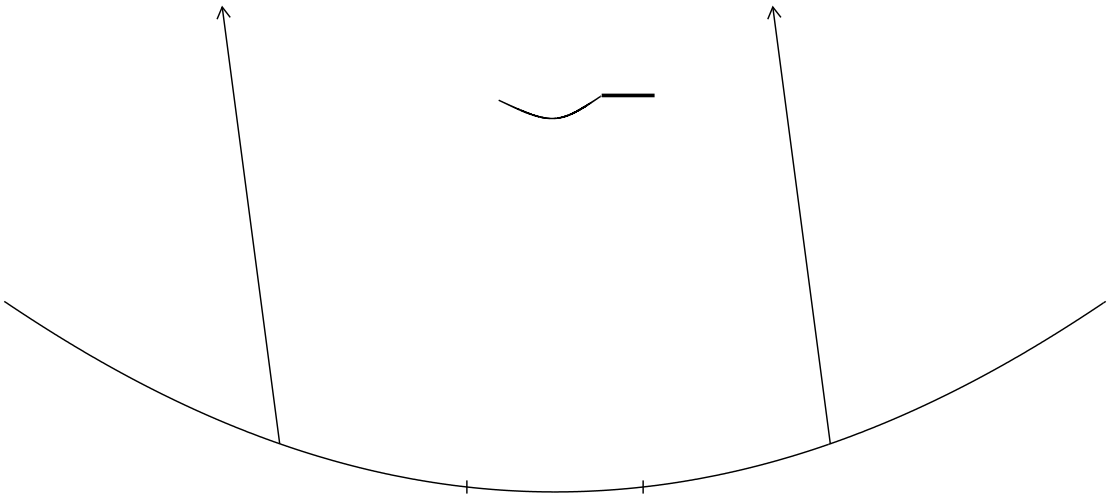

Figure 1: The side view of the VLA antenna optics. Shown also is the proposed focal plane array (thick black line next to subreflector) and the 7.2° pointing direction. The unpanelled portion of the primary is denoted by the short vertical bars.

There are many tunable parameters for such an array: shape, size, element density, location, orientation, and element type. These parameters depend heavily on each other. For example, the array size can be reduced if it can be moved closer to the best fit prime focus. Since the full phase space of possible arrays cannot be explored, I'll start with some practical constraints. For this analysis, the following are assumed:

- The focal plane array will abut the subreflector's short[1] side.
- The focal plane will lie in the plane of the best fit prime focus.
- The array will be square with regular element spacing.
- The maximum nominal frequency will be 1 GHz.
- The array will fully sample at 1 GHz (i.e., $\geq$ 15 cm spacing).

Based on the distribution of energy flux in the focal plane (see Fig. 2), an 8×8 array of 15 cm elements is considered here. Section 6.5 investigates the effects of denser arrays. This does result in about 0.4 m^2 of primary blockage (see Fig. 3), possibly justifying a deployable design. A 3D model of the antenna apex is shown in Fig. 4 with the rough geometry of the focal plane array.

4.2 Element type

We have chosen to investigate the Vivaldi slot antenna (see Fig. 5) for use as array elements. This type of antenna is well suited for this purpose for many reasons:

[1] VLA antennas have asymmetric subreflectors to illuminate offset feeds.

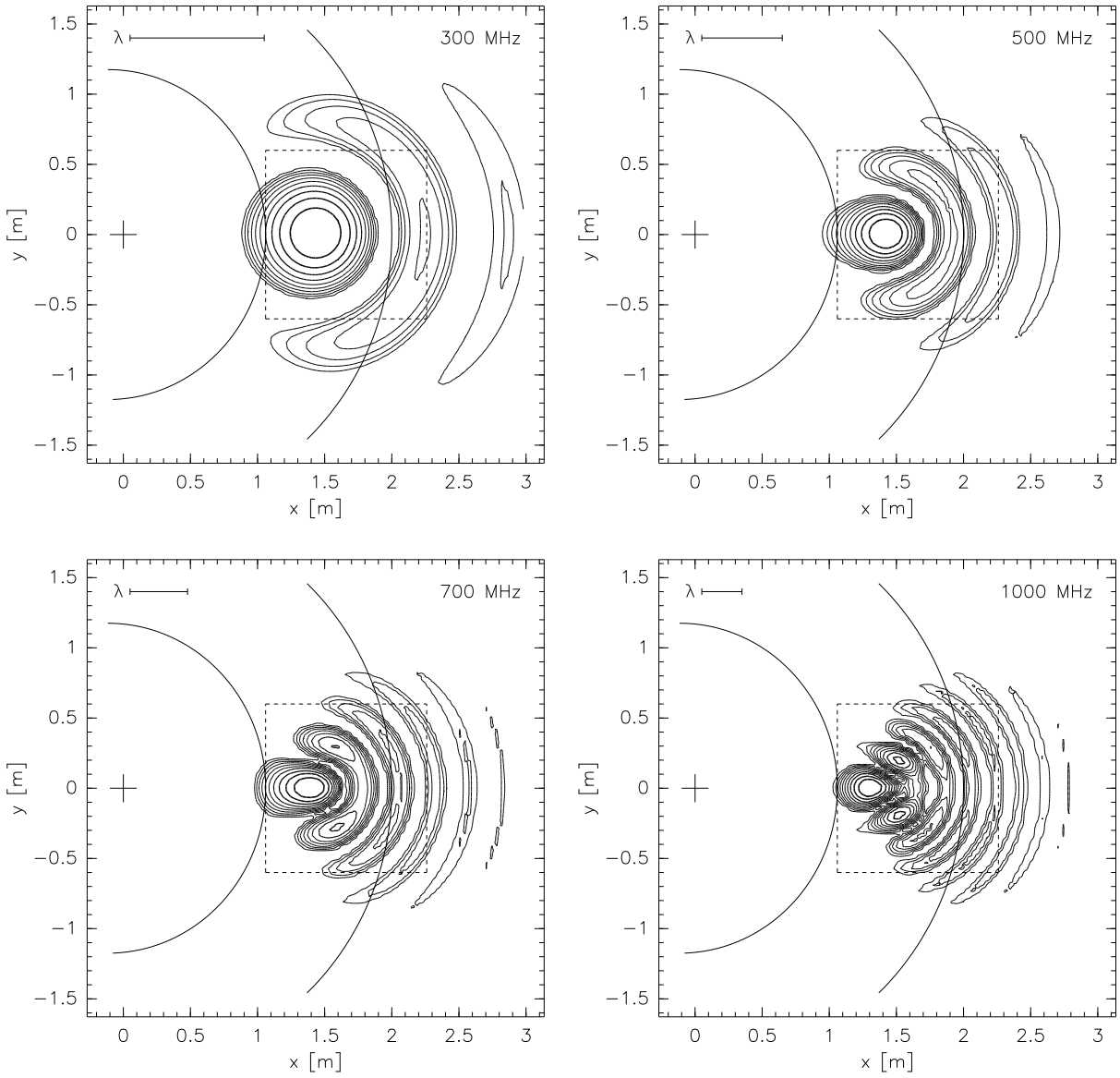

Figure 2: The electromagnetic flux penetrating the plane containing the best fit prime focus from a source 7.2° from axis for 300, 500, 700, and 1000 MHz. Contour lines show relative intensity. Each fainter contour is a factor of 1.5 lower in power. The dashed 1.2 m square is the location of the focal plane array studied here. The '+' marks the optic axis of the antenna. The semi-circle is the short side of the subreflector. The arc is the extent of the unpanelled area of the primary. The radiation source was purely circularly polarized.

- **Bandwidth** Tests by Astron have shown the Vivaldi antenna to perform well over a 5:1 bandwidth ratio [1]. A single array could be used for the entire 300 MHz to 1 GHz band.
- **Beam shape** The radiation pattern of a Vivaldi antenna when in an infinite array is almost frequency independent. Additionally, the radiation power pattern from an element is circularly symmetric with no nulls within the $\sim 70°$ view of the primary.
- **Compactness** The size of an element in an array can be far less than $\lambda/2 \times \lambda/2$, meaning the array can fully- or over-sample the impinging radiation.

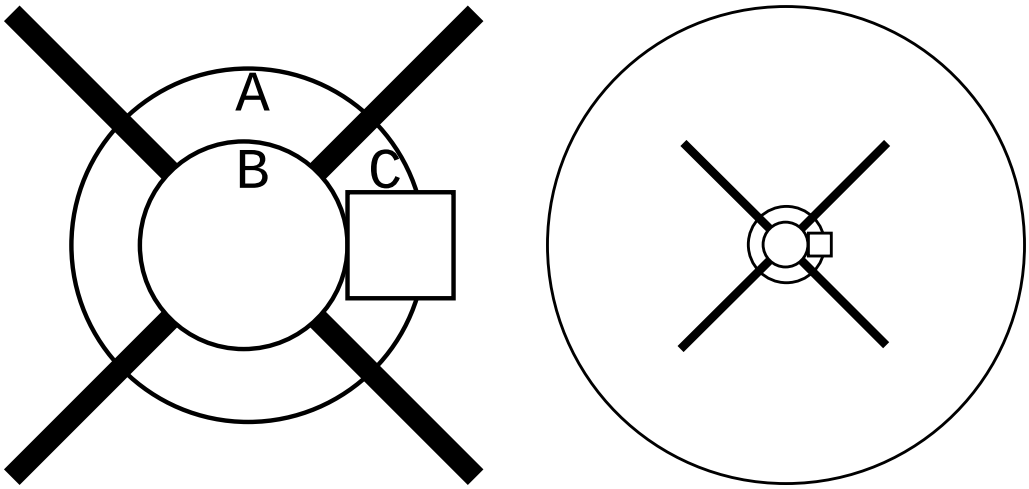

Figure 3: Location of focal plane array. *left* The focal plane array (C) is positioned close to the subreflector (B) on its short side, between support legs. A small amount of shadowing beyond the unpanelled area (A) occurs. Note that for the VLA antennas, the elevation axis is parallel to one set of support legs. In this document, figures showing the focal plane from the top will be rotated 45°. *right* The big picture. The 25 m dish as seen from the top with the focal plane to scale.

Vivaldi antennas can be easily assembled into a 2-D array. A row of elements can be printed like a circuit onto a stiff composite surface (see Fig. 6). The low noise amplifier and beam forming circuitry can be printed on the same sheet. These elements can then be assembled much like a wine box (see Fig. 7).

4.3 Vivaldi element radiation pattern

It should be stated early that due to mutual coupling, an isolated Vivaldi element behaves very differently than one in an array. An additional effect of strong coupling is that noise emitted or reflected from one element can couple into another. This noise is not dominant in realistic situations [6]. Extensive work has been done on characterizing these elements when isolated, in finite arrays, and in infinite arrays [2]. While an 8×8 array is not nearly infinite, the elements that are not on the edge of the array behave very much like ones in an infinite array. For this reason, the infinite array radiation pattern will be used at this time. Its radiation power pattern is circularly symmetric and has an electric field strength that falls off with broadside angle as

$$E \propto \left(\frac{\theta}{\theta_{\max}} \right)^{2.16} \tag{1}$$

where $\theta_{\max}$ is about 84.6°. In this approximation, no radiation is emitted beyond this angle. The gain of a Vivaldi element as a function of the broadside angle is shown in Fig. 8.

4.4 Explanation of passive and active impedences

Closely packed antennas interact with each other and there is no way of stopping it. One manifestation of this coupling is in the impedences of the devices. First imagine a single dipole antenna. Excitation of the antenna with a current will produce radiation. The impedence of this single antenna, Z is as defined by Ohm's law as the ratio of voltage V to current I in the feed, and can be complex if the two values are out of phase. In the absense of resistive losses, the impendence of the system can also be related to the total radiated power P of the antenna, $\Re Z = P/|I|^2 = |V|^2/P$. Now consider two parallel, identical dipole antennas that are placed very near each other $d \ll \lambda$. In fact, make them practically touch. If the currents in the two antennas are equal, at a value I each, this would be equivalent to a single dipole, with total impedence Z and a current $2I$. Thus the effective impedence of each dipole must be $2Z$. If the currents are

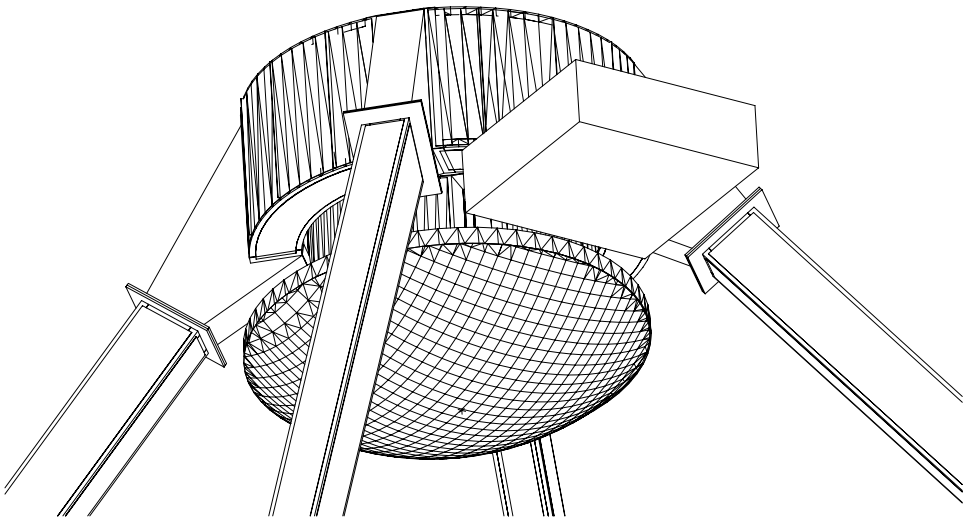

Figure 4: A 3D view of the antenna apex. The focal plane array is represented by the nondescript box.

equal and opposing, then no power would be radiated. Thus the impedence is zero. A low voltage differential signal (LVDS) cable takes advantage of this property of not radiating by sending opposing currents down parallel lines, thus improving its own immunity to interference and preventing interference to other devices. This impendence that depends on the phases and amplitudes of the currents at each of the other elements is the active impedence. The example of nearly coexisting dipoles is an extreme case. The active impedences determine the voltages produced at the array elements when exposed to radiation.

Return to that LVDS cable, or a coax cable, for a moment. We all remember that these cables have characteristic impedences, typically around 50Ω. This impedence is equal to the amount of termination required to prevent signal reflection at its end. Maximizing the transmitted power requires matching the impedence of the cable with the impedence of the device begin connected. Likewise, the performance of an antenna depends on the match of the feed to the amplifier that follows. An imperfect match between the feed and amplifier will reduce the power transmitted (and hence the sensitivity of the antenna) and increase the noise figure of the amplifier. The reflected power has potential to be a source of coherent noise to the other elements in the array. The magnitude of this effect is unknown, especially in the focal plane situation where each element is weighted differently. This matching impedence is called the passive impedence and is equal to the impedence of of an element when all of the other elements in the array are properly terminated. A difficulty in matching results when the passive impedences are frequency dependent. In the case of antennas, the passive impedence is often not purely resistive.

5 A physical optics model

The detailed analysis of a VLA antenna at frequencies below about 1 GHz requires the use of physical, rather than geometric, optics. At least two methods of solving fields in electromagnetic systems are frequently used. The Method of Moments (MoM) self-consistently solves for the fields on all surfaces, requiring inversion of large matrices. For the VLA antenna at 1 GHz, these matrices exceed a size of 60000×60000, making this $\mathcal{O}(n^3)$ algorithm unsuitable. MoM was used by others to compute the properties of Vivaldi arrays. Instead of MoM, perturbative diffraction is used here. In this method, the electromagnetic field due to each surface is computed by integrating the Kirchoff integrals over each of the other surfaces. Higher orders in the perturbative expansion can be achieved by recomputing the Kirchoff integrals with the fields computed by the previous iteration. The complexity is $\mathcal{O}(n^2)$ per iteration, making it tractable for larger systems. In the cases encountered here, only the first order perturbations are required as the convergence is quite rapid.

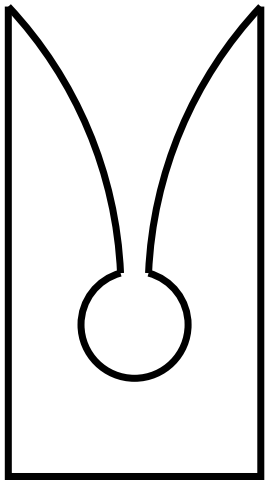

Figure 5: A single Vivaldi element. The depth of an element is roughly twice to three times that of its width. A field probe is placed near the circular cavity.

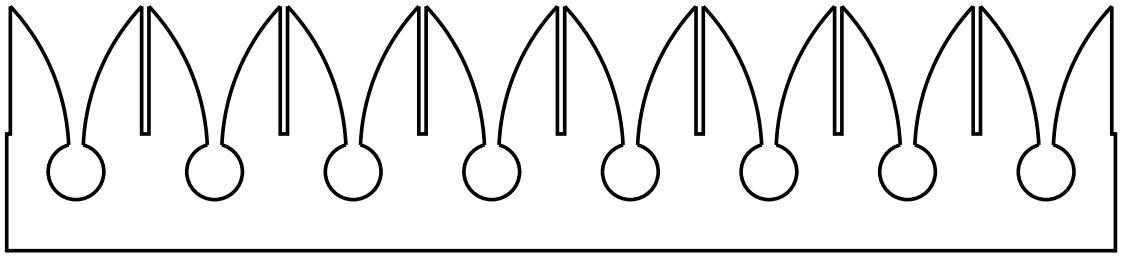

Figure 6: Eight Vivaldi elements can be printed onto one sheet of composite. 18 sheets (9 as above and 9 with the inter-element notches cut from the bottom) can be assembled into a single dual-polarized array of elements. The resultant array has 8×9 elements of each linear polarization.

6 Getting the most out of the array

6.1 Array placement

The array should be placed so that it maximizes the received power. This is not the proper figure of merit to evaluate the performance of the array, but it serves as a convenient starting point. The ratio of gain to system temperature will be the final metric. To determine the focal plane power density, the primary was illuminated by a point sources at the appropriate 7.2° angle from axis. This angle was determined by requiring that the best focus lie a half beam-width outside the subreflector's short side. The fields on the primary are then diffracted onto the focal plane. The energy flux is computed by constructing the Poynting vector at each position on the plane and taking its dot product with the focal plane normal vector. The flux distributions for four selected frequencies are shown in Fig. 2. Between 72% and 77% of the energy flux intercepts the 1.2 m square focal plane array. The absence of the support legs in this analysis certainly biases toward higher efficiency. Focal plane arrays are likely to cope better with the effects of the legs because of their adaptability.

6.2 Weight optimization

The RF output of the phased array is a complex-weighted sum of the individual element outputs. In principle, an arbitrary number of phased outputs could be constructed, however in practice, between 1 and 4 phased

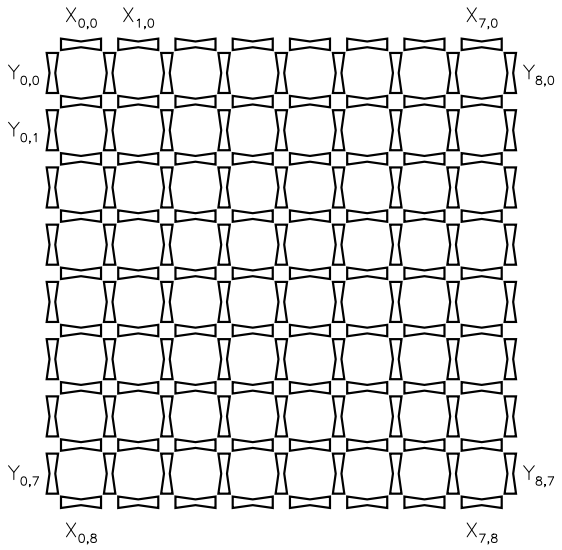

Figure 7: The top view of an assembled 8×8 cellarray. The 72 vertical elements form one polarization array and the 72 horizontal elements form the other. Note that elements of opposite polarization are not collocated. $X_{0,0}$ designates the top left element of X polarization.

outputs per polarization are likely. The sum for each polarization could in principle include contributions from both polarizations to account for the slight rotation of polarization across the focal plane. This effect is small, so the inclusion of both polarizations into the phased sum will be omitted here.

The modern metric for evaluating the performance of an antenna is $G/T_{\rm sys}$, the ratio of the forward gain to the system temperature. This is a measure of the sensitivity in the direction of maximum gain. While this metric doesn't explicitly favor a symmetric beam with minimal sidelobes, the resultant beam is often fairly good. In this section, optimization at a given frequency with infinitesimal bandwidth is described. Simultaneous optimization over a useful bandwidth is deferred to a later document.

This optimization is achieved by solving for a complex weight vector, $\vec{w}$, which maximizes the expression:

$$\frac{G}{T_{\rm sys}} = \frac{\vec{w}^{*\rm T} \cdot \mathbf{G} \cdot \vec{w}}{\vec{w}^{*\rm T} \cdot \mathbf{T} \cdot \vec{w}} \tag{2}$$

Where the gain matrix, $\mathbf{G}$, and the temperature matrix, $\mathbf{T}$, are Hermitian. $\mathbf{G}$ is computed by illuminating the primary with the Vivaldi array with pairs of elements active. The matrix elements are derived from the Poynting flux in the source direction. $\mathbf{T}$ is computed by illuminating a surface that encloses the focal plane array, with the primary omitted. The Poynting flux through this surface is computed. If the Poynting vector is downward directed, it contributes to ground spillover, which sees 300K. Otherwise it contributes toward sky spillover. The sky temperature is assumed to be

$$T_{\rm sky}[\rm K] = 3 + 3\,\nu[\rm GHz]^{5/2} \tag{3}$$

In addition to temperature contributions from the sky and ground, a contribution due to the receiver temperature is added. A conservative value of 50K was used for this. According to industry projections, low noise amplifiers using CMOS technology could achieve noise temperatures of 20K by the year 2010 at quite affordable prices. Resistive losses and imperfect matches will also contribute to the receiver temperature.

Each component of the weight vector is proportional to the current of its respective focal plane array element. Since the elements on the array are strongly coupled, they each have different frequency dependent impedances meaning that the power emitted, speaking from the transmission point of view, is not simply proportional to the sum of the squared currents. A third matrix, $\mathbf{Z}$, is also computed which allows the total power to be computed:

$$P \propto \vec{w}^{*\rm T} \cdot \mathbf{Z} \cdot \vec{w}. \tag{4}$$

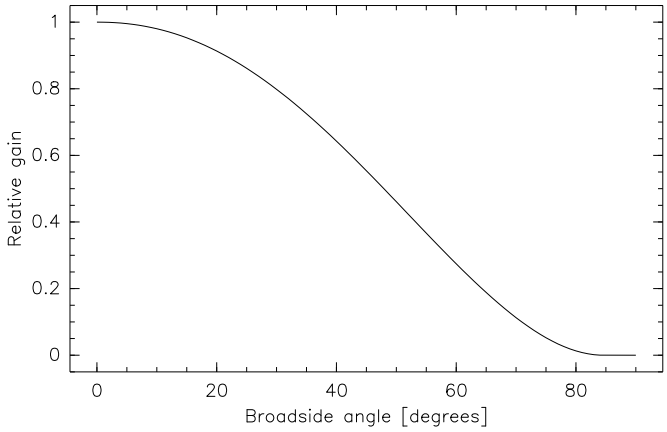

Figure 8: The gain of a single Vivaldi element within an infinite array as a function of the broadside angle. The gain is independent of the azimuthal angle and of frequency.

This matrix is needed to compute G and $T_{\rm sys}$ in an absolute sense. An focal plane array composed of widely separated elements would have a trivial $\mathbf{Z}$ matrix. The $\mathbf{Z}$ matrix turns out to be the active impedance matrix. This derives from requiring that for each pair of elements that the output power is proportional to the current squared multiplied by the impedance. Thus, the voltages corresponding to weight (current) vector $\vec{w}$ are simply $\mathbf{Z} \cdot \vec{w}$. The array phasing is done by summing weighted voltages, making the voltage basis more natural than the current basis. The calculations are more easily performed using the current basis because $\mathbf{Z}$ can have eigenvalues that differ by factors of 10^7 or more. This makes the inversion of $\mathbf{Z}$, and hence the construction of the voltage-basis versions of $\mathbf{G}$ and $\mathbf{T}$, numerically unstable, especially in highly oversampled conditions.

6.3 Optimization results

This section summarizes the results of the $G/T_{\rm sys}$ optimization for a VLA antenna with the above mentioned focal plane array. In Fig. 9 several performance parameters are plotted against frequency for optimization with infinitesimal bandwidth. Note the substantial decrease in efficiency as the frequency increases above 600 MHz. This is likely due to the elements sampling over a finite sized region in the focal plane. Decorrelation starts to occur as the frequency increases due to the fields changing substantially over distances on the order of the element size. This was confirmed by rerunning the optimization on an array of the same physical size consisting of 10×10 cells. Parameters for 300, 500, 700, and 1000 MHz are given in Table 1. The weight vectors resulting from optimization are shown in Fig. 10. Plots of the illumination of the primary are shown in Fig. 11. Plots of the resultant beams are in Fig. 12.

Freq. (MHz)	G (dBi)	$T_{\rm sys}$ (K)	$G/T_{\rm sys}$ ($\rm K^{-1}$)	efficiency (%)	max sidelobe (%)
300	36.9	117.2	41.8	77	4.3
500	41.2	73.6	181.1	77	3.6
700	44.0	63.5	396.9	75	3.3
1000	46.4	58.4	740.6	63	4.9

Table 1: Parameters of optimized array for four selected frequencies. Since blockage due to the legs has been ignored at this point, the efficiency listed here is artificially high.

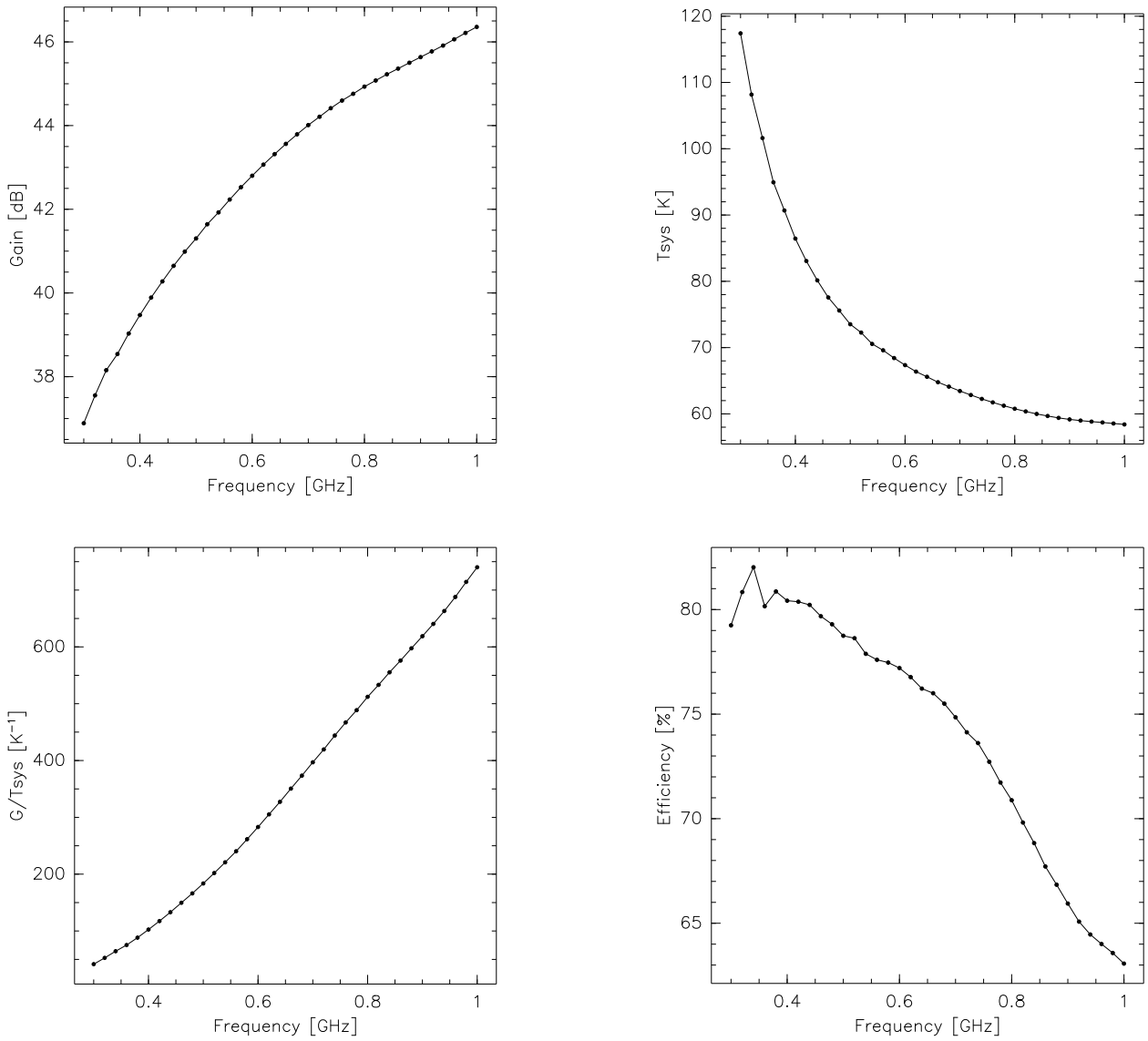

Figure 9: Performance figures for infinitesimal bandwidth optimizations.

6.4 Prime focus performance

In order to judge the performance hit taken by placing the array off of the best fit prime focus, an identical array, centered on prime focus, was simulated. This is only practical on VLA antennas with an FRRM subreflector mount that allows access to prime focus. The performance of this array is shown in contrast to the array studied in more detail in Fig. 13.

6.5 The effect of a denser array

The 8×8 cell array studied in detail critically samples the impinging radiation at 1000 MHz. The illumination pattern at 1000 MHz (see Fig. 11) shows that optimal performance is not being reached at this frequency. Simulations were run for denser grids of the same physical size. They showed substantial performance increases, especially at the higher frequencies (see the dotted lines and diamonds as compared to the solid lines in Fig. 13). It is still unclear to me why the illumination patterns are asymmetric, although the

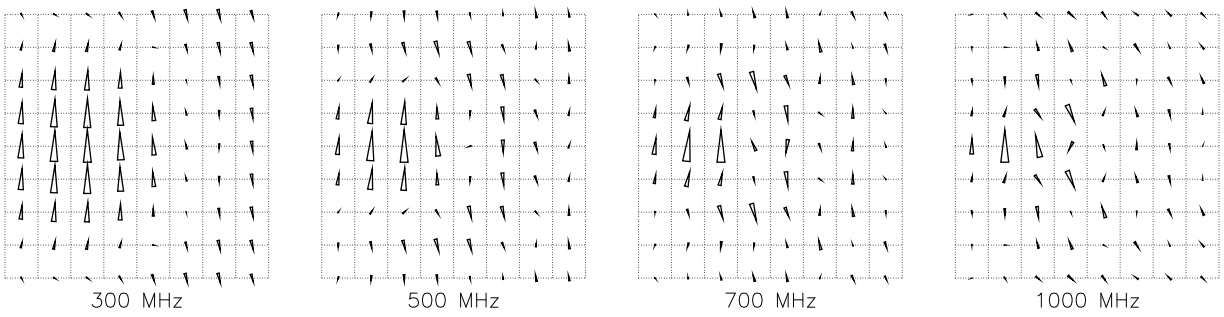

Figure 10: The element weights produced by optimization of $G/T_{\rm sys}$. These weights applied to the voltages of their respective elements produce the optimal output. For each plot, the weights are scaled such that the weight with the greatest magnitude is scaled to a length of 1 cell and points up. The weight phase is equal to the angle that the arrow is rotated. Note that the amplitudes very nearly match the power density in the focal plane shown in Fig. 2.

asymmetries get less severe as the element density increases. Arrays with more elements behave more like infinite arrays, making the infinite array approximation more approriate as well. Cost and complexity will increase with the number of elements. The low frequency performance might suffer more as the elements become smaller. If the performance becomes too miserable at the lower frequencies, a second focal plane array for $\sim$ 200 to 500 MHz may be justified.

7 Comparison with other concepts

7.1 GBT low frequency feeds

The GBT uses 5 receivers to cover the 290 to 1230 MHz frequency range. The three lowest frequency feeds are dipoles while the other two are corrugated horns. Table 2 summarizes the performance of these receivers. All five of these use low noise amplifiers that are cooled to 15K. It is unlikely that the focal plane array being studied here can be cooled.

Freq. (MHz)	est. $T_{\rm sys}$ (K)	$T_{\rm rec}$ (K)
290-395	30	9-16
385-520	30	12-17
510-690	30	10-12
680-920	25	9-30
910-1230	25	?

Table 2: Performance of the GBT low frequency feeds. All of this information can be found on the GBT prime focus receiver web page [4].

8 Bandwidth issues

The focal plane array discussed here will probably be limited in usefulness mostly by bandwidth. Many factors contribute to difficulties in exploiting the full bandwidth of the Vivaldi array.

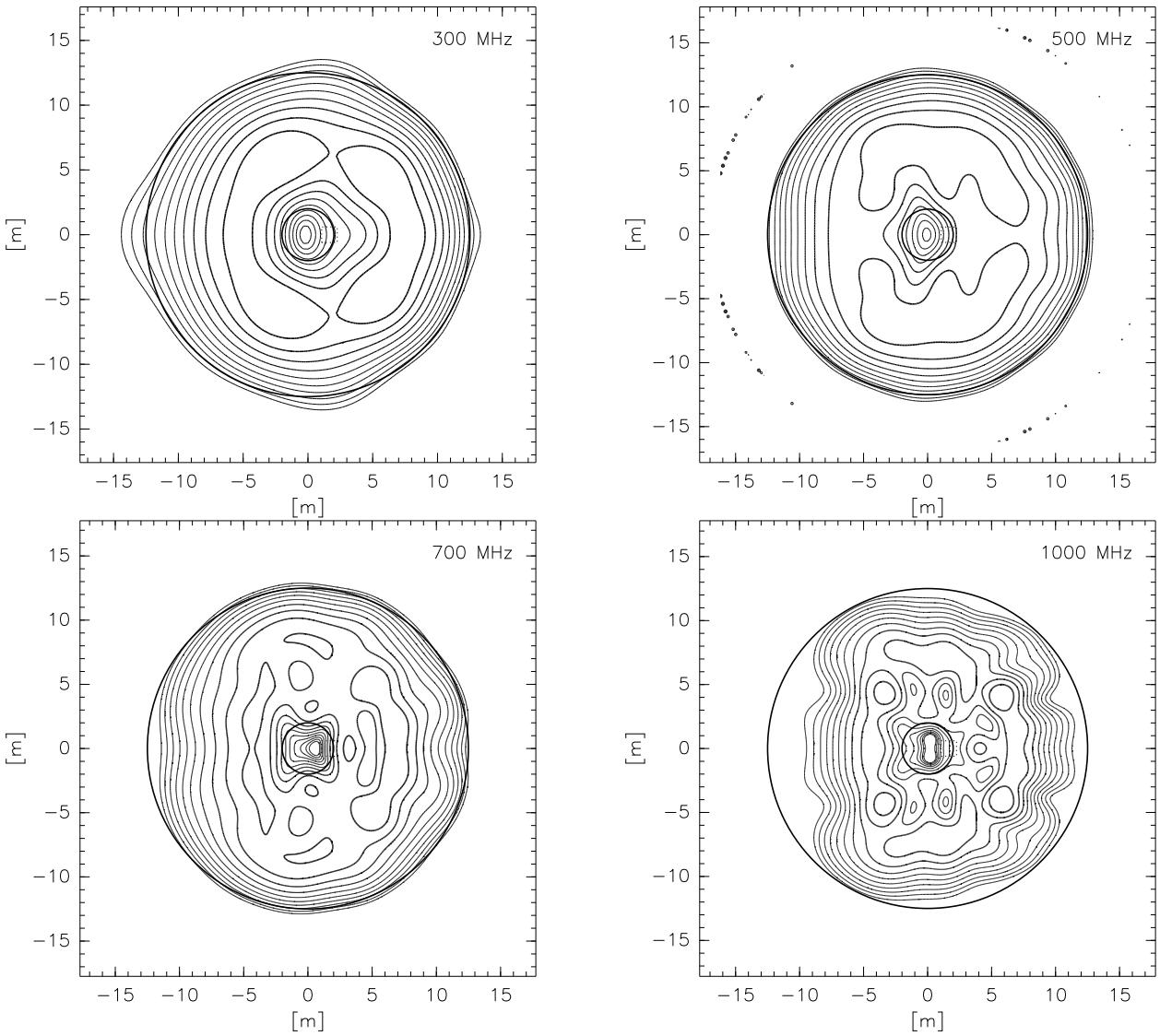

Figure 11: Dish illumination for the Vivaldi array optimized at 300, 500, 700, and 1000 MHz. The contours represent the field strength (power) on the primary. The outer dark circle is the edge of the 25 m dish. The inner dark circle represents the unpanelled area. Each contour represents a factor of 1.5. Note that the unpanelled area is generally illuminated less.

8.1 Frequency-dependent weights

For optimal performance, the phasing weights must change with frequency. Fig. 2 shows the power density across the focal plane. The voltage weight amplitude for a given element is nearly proportional to the power density at its location. While the weight very near the center of the main power lobe changes little with frequency, the weights of the elements far from the main power lobe change rapidly with frequency (see Fig. 17). For this reason, the efficiency of a the array must decrease with increased bandwidth when a single set of weights is used. A 100 MHz bandwidth will probably be possible with acceptable performance across the band.

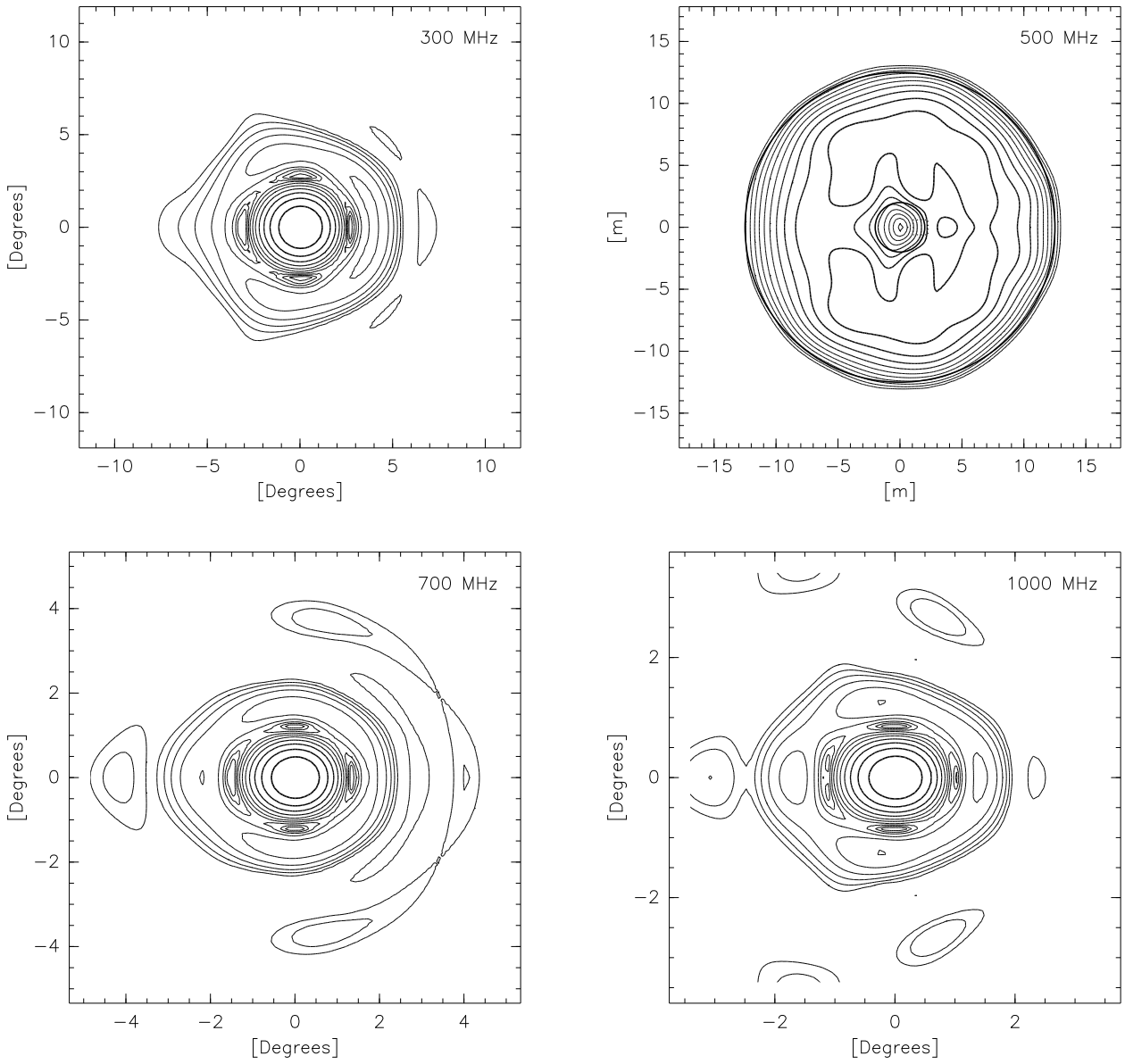

Figure 12: The beams at 300, 500, 700, and 1000 MHz. Each fainter contour represents a factor of 2.0 decrease in gain. The greatest sidelobes are less than 5% in all cases.

8.2 Matching the elements

One unfortunate aspect of Vivaldi arrays is the variability of the antennas' impedances. The passive resistance can vary from $R = 30\Omega$ to 190Ω and the passive reactance ranges from $X = -50\Omega$ to 100Ω across the 300 to 1000 MHz band that we are considering [3]. The majority of the excursions from the typical values of $R = 100\Omega$ and $X = -40\Omega$ occur in the lower part of the band. Since the low noise amplifiers perform very well only for a signal with the appropriate impedence, the system temperature will vary across the band. In order to mesh best with the low end of the L-band, any matching will be optimized for the 1000 MHz end of the band. Lengthening the elements leads to improved passive impedence properties [6].

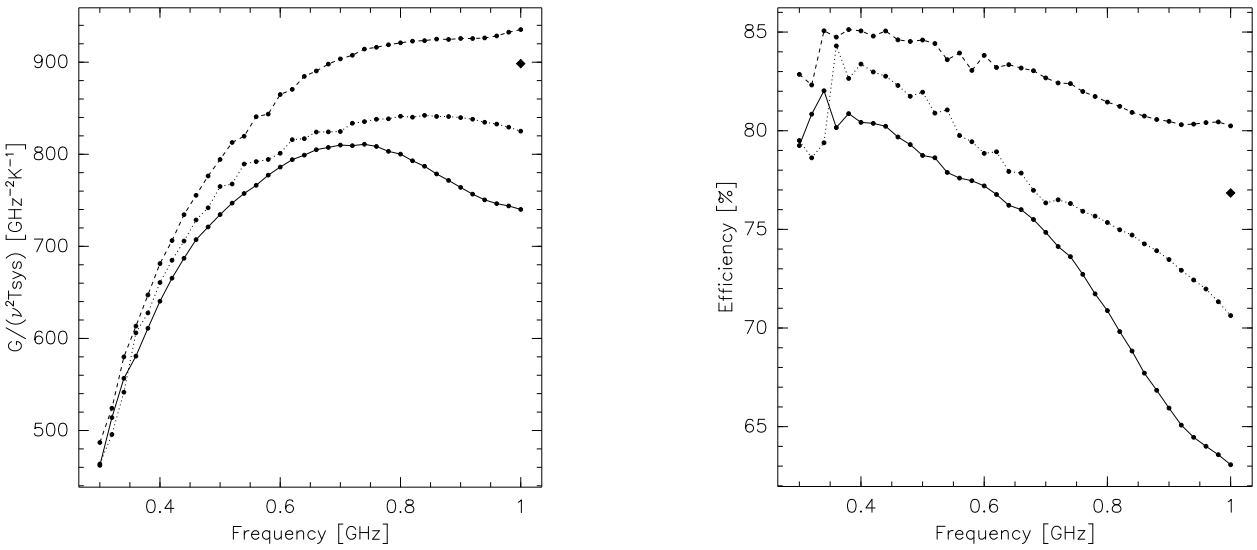

Figure 13: $G/\nu^2 T_{\rm sys}$ and efficiencies for three array models. The solid lines are the same as in Fig. 9, corresponding to an 8×8 cell array of 15 cm elements placed next to the short side of the subreflector. The dotted lines correspond to an array composed of 10×10 cells, each 12 cm on a side (covering the same area). The dashed lines correspond to an 8×8 cell array of 15 cm elements, but instead centered on prime focus. The diamond symbol represents performance at 1 GHz for a focal plane array next to the subreflector consisting of a 15×15 cell array of 8 cm elements. Note that the calculations below 400 MHz suffer from some numerical instabilities due to the high degree of oversampling at these low frequencies. Thus the ripples in the efficiency curves are likely not real.

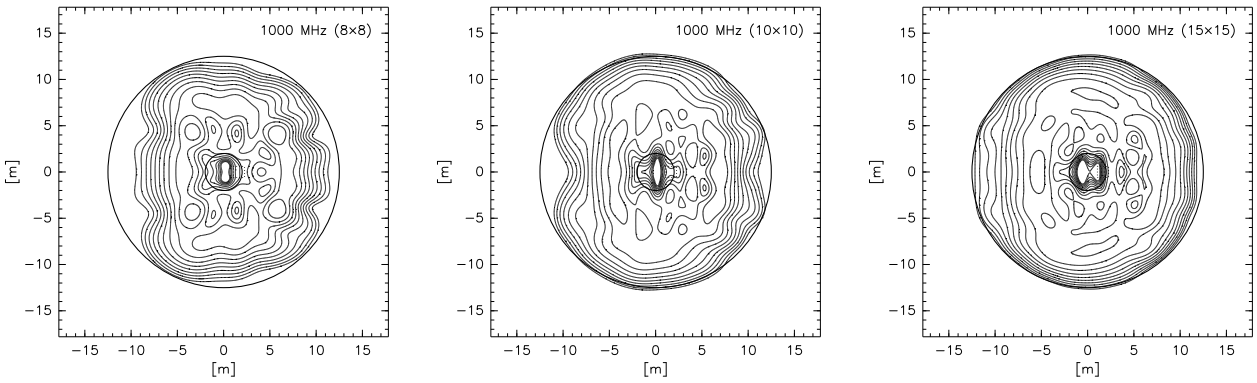

Figure 14: Primary dish illumination at 1000 MHz for a 1.2 m square arrays with different element densities. The left plot is for the 8×8 array of 15 cm cells. The center plot is for a 10×10 array of 12 cm cells, and the right plot is for a 15×15 array of 8 cm cells. Note the improvement in illumination as the element density increases.

8.3 Forming the beam(s)

Beam-forming within each antenna's focal plane array will most certainly be done with analog electronics. While digital beam-forming certainly has advantages, such as better stability and greater flexibility in weighting, extreme costs rule it out immediately. Fully digitizing each element would cost close to \$1M per VLA antenna. Even digitally sampling 100 MHz of bandwidth from each element is cost prohibitive. Analog beam-forming was successfully used in the Thousand Element Array (THEA) [5]. This array was a technol-

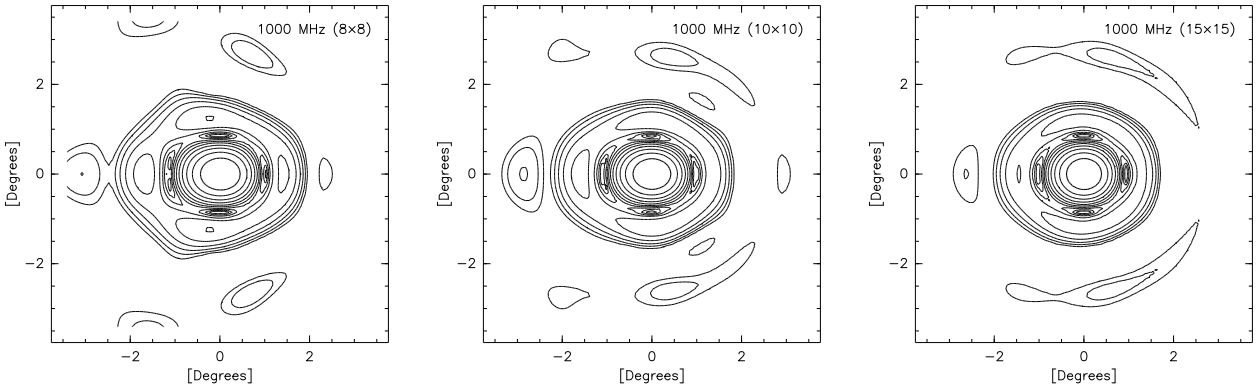

Figure 15: Beam patterns at 1000 MHz for a 1.2 m square arrays of different densities. Each plot here corresponds to one plot in Fig. 14

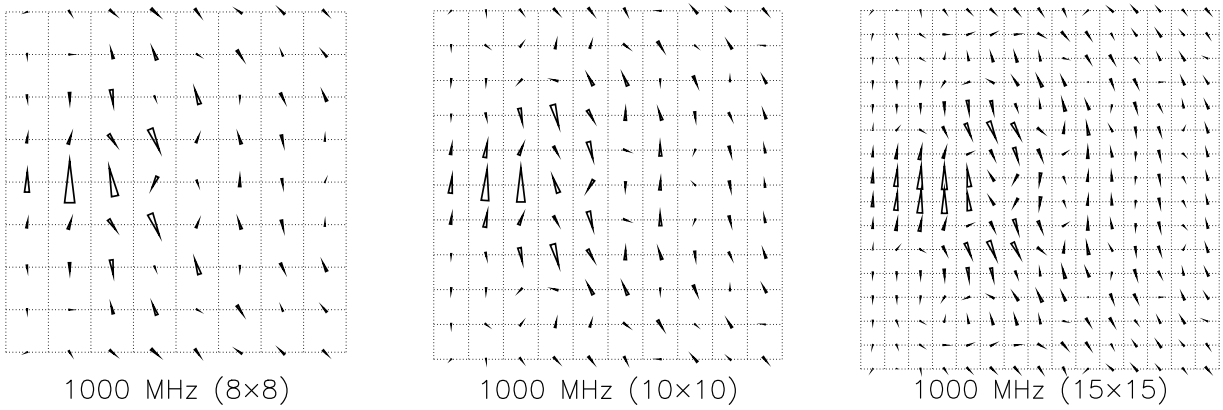

Figure 16: Weight vectors at 1000 MHz for a 1.2 m square arrays of different densities. Each plot here corresponds to one plot in Fig. 14

ogy demonstrator built by Astron as part of their SKA effort. Each of their 64 element, single polarization arrays was able to produce two phased RF output beams. One option to improve the bandwidth for the EVLA application is to provide multiple phased outputs, each optimized for a different frequency range. Multiple phased outputs could potentially be used to provide multiple beams on the sky. In this case, the weights would need to be updated to accomodate the changing parallactic angle.

9 Additional issues

Briefly, I mention some things that may complicate the focal plane solution, or any other solution, to the low frequency problem:

- **New Mexico Array antennas, PT, LA** *Ignoring the LA situation* the completion phase of EVLA will involve building about 8 new antennas and incorporating the PT and LA VLBA antennas. PT and LA have larger subreflectors, potentially making the focal plane array less effective. It is presumed that the NMA antenna optics will likely resemble the VLA optics in order to accomodate the feeds being designed for EVLA. Outfitting PT and LA may prove to be difficult.

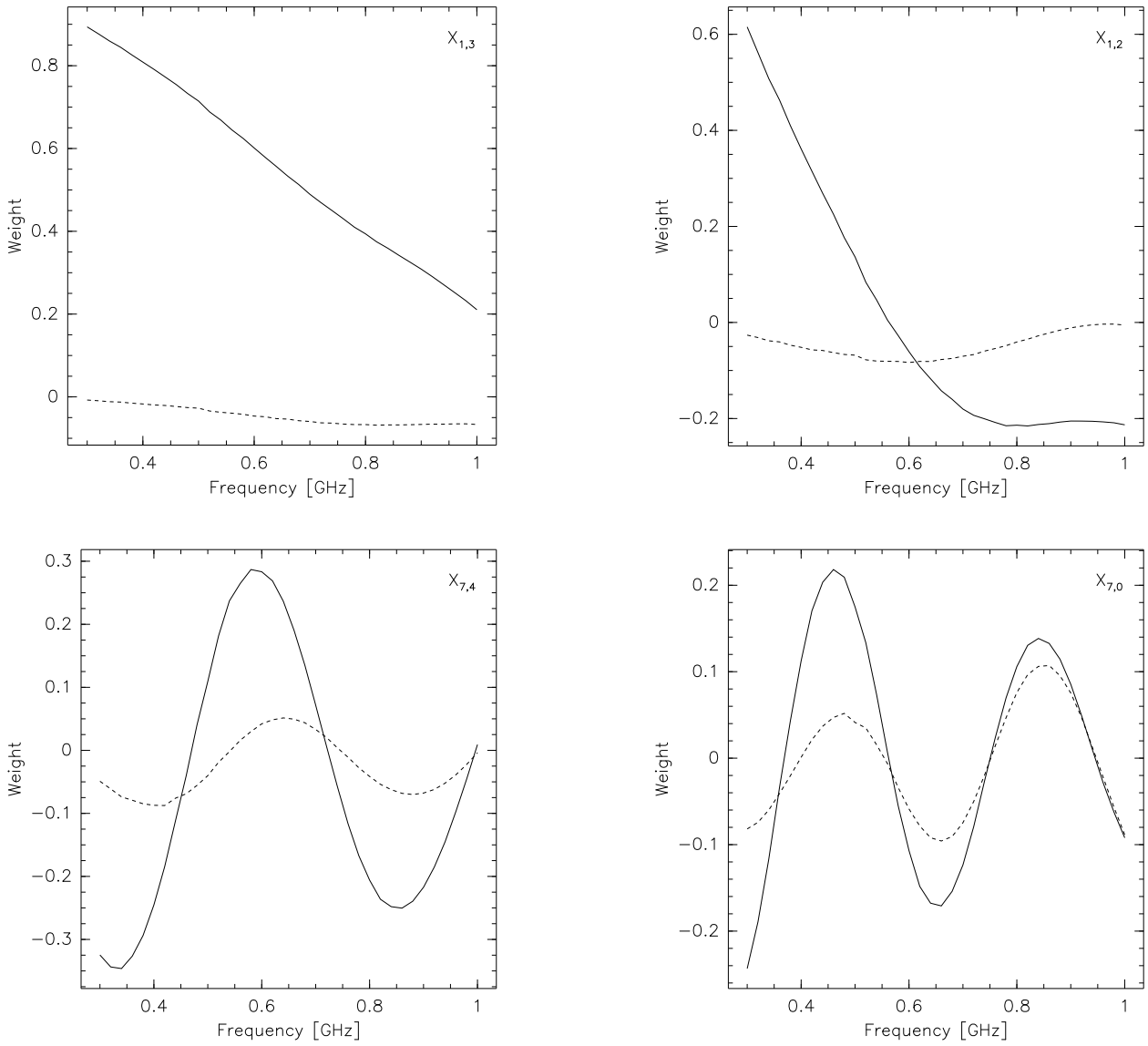

Figure 17: The phasing weights as a function of frequency for elements $X_{1,3}$, $X_{1,2}$, $X_{7,4}$ and $X_{7,0}$. See Fig. 7 for element nomenclature. The solid line shows the real part of the weight and the dashed line is for the imaginary part. Note that the weight variability increases with distance from the best fit focus, which is between elements $X_{1,4}$ and $X_{2,4}$.

- **Finite bandwidth** The above simulations and optimizations are for a single frequency. For the focal plane array to be a viable option, a substantial output bandwidth is needed. While the Vivaldi array is inherently a wide band device, there are two effects which will limit the simultaneously useful bandwidth. The first is that the weights appropriate for one frequency will certainly not be appropriate for another. The second is that the active impedance of each element is frequency dependent making the matching of the device impedance with its load difficult.

- **Legs** The quadrupod structure (legs) contribute to about 8 m^2 of plane wave blockage (seen by the source). They also contribute to a similar amount of spherical wave blockage (seen by the array). Electrically, the legs appear to be about $\lambda/2$ in diameter. The effects of the legs will likely be included in the next version of this document.

- **Polarization** While the code used to compute fields and optimize weights is fully capable of handling arbitrarily polarized sources, little work has been done on exploring the polarization characteristics of the array. It is anticipated that the familiar effects of beam squint will be present, however, dual-polarization optimization may allow them to be minimized. It is likely that circular polarization is desirable for the lower frequency bands since then the effects of Faraday rotation are solely in phase, simplifying calibration greatly. The array most naturally produces linear polarization, so this may cause some additional difficulty. Conversely, the flexibility of the array may allow D-terms to be minimized by the tweaking of weights, at least over a small bandwidth.
- **Lightning** The focal plane array will likely use sensitive, high input impedance amplifiers which are very sensitive to static discharge. Also the placement of the array will make it a likely target for lightning hits.
- **Lower frequencies?** A 74 MHz dipole is occasionally installed at the VLA. While this system is only about 15% efficient, the science it produces is unique and important. It would be nice to retain this capability, or better yet to improve on it. This would likely be implemented as a separate device.

10 Acknowledgments

Many thanks go to Christophe Craeye for assistance through several email exchanges. Jim Ruff provided the 3-D view of the apex area.

References

[1] J. G. Bij de Vaate, G. W. Kant, W. A. van Cappellen, & S. van der Tol, "First Celestial Measurement Results of the Thousand Element Array", URSI GA, Maastricht, August 2002

[2] C. Craeye, A. O. Boryssenko, & D. H. Shaubert, "Analysis of infinite and finite arrays of tapered-slot antennas for SKA", Proc. of the 2002 European Microwave Conference," pp. 1003-1006, Milano, Sept. 2002.

[3] Craeye C., Arts M.J., Bregman J.B., "Truncation effects in tapered-slot antenna arrays for radio astronomy applications," Proc. of the URSI Symposium, Maastricht, The Netherlands, Aug. 2002.

[4] GBT Prime Focus Receivers, `http://www.gb.nrao.edu/~fghigo/gbtdoc/prime.html`.

[5] J. G. Bij de Vaate, "The Thousand Element Array, Results of a demonstration project", SKA Workshop presentation, 2002

[6] C. Craeye, private communication.